

## Article

# Dynamical Analysis and Finite-Time Synchronization for a Chaotic System with Hidden Attractor and Surface Equilibrium

Runhao Zhang <sup>1</sup>, Xiaojian Xi <sup>1</sup>, Huaigu Tian <sup>1</sup>  and Zhen Wang <sup>1,2,\*</sup> 

<sup>1</sup> Xi'an Key Laboratory of Human-Machine Integration and Control Technology for Intelligent Rehabilitation, School of Computer Science, Xijing University, Xi'an 710123, China

<sup>2</sup> Shaanxi International Joint Research Center for Applied Technology of Controllable Neutron Source, School of Electronic Information, Xijing University, Xi'an 710123, China

\* Correspondence: wangzhen@xijing.edu.cn

**Abstract:** In this paper, a chaotic system with surface equilibrium and a hidden attractor was studied, and the dynamical behavior, synchronization scheme and circuit application of the system were analyzed. Firstly, the stability analysis and dynamic behavior of the system were carried out (the type of attractor, bifurcation, Poincaré section, Lyapunov exponents spectrum and complexity). Secondly, the finite-time synchronization observer was designed according to the finite-time stability theorem to achieve the synchronization of the finite-time master–slave systems, and the error system asymptotically approached zero. Finally, the existence and practicability of the original system were proven through the implementation of the circuit system, and through using an appropriate control circuit to realize the synchronization of chaotic master–slave systems.



**Citation:** Zhang, R.; Xi, X.; Tian, H.; Wang, Z. Dynamical Analysis and Finite-Time Synchronization for a Chaotic System with Hidden Attractor and Surface Equilibrium. *Axioms* **2022**, *11*, 579. <https://doi.org/10.3390/axioms11110579>

Academic Editors: Eric Campos-Cantón, Ernesto Zambrano-Serrano, Guillermo Huerta Cuellar and Esteban Tlelo-Cuautle

Received: 28 September 2022

Accepted: 20 October 2022

Published: 22 October 2022

**Publisher's Note:** MDPI stays neutral with regard to jurisdictional claims in published maps and institutional affiliations.



**Copyright:** © 2022 by the authors. Licensee MDPI, Basel, Switzerland. This article is an open access article distributed under the terms and conditions of the Creative Commons Attribution (CC BY) license (<https://creativecommons.org/licenses/by/4.0/>).

**Keywords:** surface equilibrium; hidden attractor; finite-time synchronization; circuit implementation

## 1. Introduction

Simple nonlinear differential equation systems can exhibit chaos, which is a universal phenomenon in nonlinear systems, and there is a large amount of evidence that chaos exists in reality [1]. In 1963, while designing a 3D model of atmospheric convection, Lorenz constructed a 3D quadratic polynomial ODE system in which he discovered the first chaotic attractor [2]. Later, many Lorenz-like systems, such as Sprott [3], Chen [4] and Lü [5], were constructed and studied, and studies of these systems also inspire us to think deeply about Lorenz-like systems. After Leonov put forward the mathematical definition of a hidden attractor [6], the research theory and application of a hidden attractor have been widely concerned [7], where the attraction domain does not intersect with the neighborhood of any unstable equilibria, and the basis of attraction is small for such systems [8,9]. Chaos cannot be excited by arbitrarily choosing the initial conditions near the unstable equilibria. Hence, the occurrence of hidden attractors in the system is not obvious and is difficult to be noticed [9]. Recently, chaotic systems with various equilibria have also been considered under the category of hidden attractors [10]; this includes systems with only one stable equilibrium [11,12], without an equilibrium [13,14] and with infinite equilibria [15–17]. There is a significant correlation between hidden attractors and multistability, which is a very important phenomenon in dynamic systems [18,19]. In fact, it is difficult to discover hidden attractors in physical systems as the systems themselves have specific physical properties that cannot be arbitrarily changed [20]. Meanwhile, hidden attractors are potentially harmful to engineering. Therefore, finding hidden attractors and identifying the dynamics of these system is challenging work. Moreover, chaotic systems with hidden attractors may have richer complex behavior than the self-excited attractors, so it is more helpful for the application of electronic circuits, artificial intelligence and so on [21–23].

The synchronization control of chaotic systems is also a classical and major topic of discussion in the field of nonlinear control [24–26]. For the actual chaotic systems, there are often some characteristics, such as various disturbances and uncertainties in the system, and the chaotic phenomenon is extremely sensitive to the initial value and parameter variation. Hence, using control strategies to achieve the synchronization control of uncertain chaotic systems with unknown parameters is still a challenge for some engineering applications, and this research is still an important and difficult problem to be urgently solved. For the uncertain chaotic synchronization control problem with unknown parameters, the dynamics and robustness of the master chaotic system following the slave chaotic system are key to measuring the synchronization performance. Aiming at this goal, researchers have proposed and verified many control methods: adaptive feedback synchronization control [27–30], sliding mode variable structure control [31–33] and robust control [34]. With the deepening of theoretical research, the methods of control are tending to maturity. Therefore, the research trend of chaotic synchronization will be how to realize the synchronization of chaotic systems with a simple structure, small control amount and finite time. Finite-time synchronization technology was first proposed by Haimo [35]. Yu [36] and Amato [37] proposed the concept of global robust terminal sliding mode control for a single input single output (SISO) of an uncertain nonlinear system and presented the design method of the controller. Then, finite-time synchronization control was applied to various engineering fields, including chaotic systems [38–40]. However, the parameters of chaotic synchronization used in practical engineering are variable and unknown, so the assumption of the above methods tend to be idealized. Meanwhile, there are few studies on the finite-time synchronization of chaotic systems with hidden attractors. Only when the synchronization error of the system converges in finite time and the control has strong robustness can it have a more practical engineering value. Thus, for the unique mechanism of chaotic systems with hidden attractors, the design of finite-time observers provide inspiration for solving the problems of sudden oscillations caused by hidden attractors. In this paper, we further elaborate on a chaotic system with surface equilibrium and a hidden attractor [41]:

$$\begin{cases} \dot{x}_1 = x_1x_2^2 + ax_1^2x_2 \\ \dot{x}_2 = -x_1x_3 \\ \dot{x}_3 = bx_1 + x_1^2x_2 \end{cases} \tag{1}$$

where  $x_1, x_2$  and  $x_3$  are state variables of the system and  $a$  and  $b$  are parameters of the system. In this paper, the structure is as follows: in Section 2, the dynamical behavior of a chaotic system is analyzed, such as equilibria analysis, periodic orbit, Poincaré map, Lyapunov exponents spectrum (LEs), largest Lyapunov exponent (LLE), bifurcation diagram and complexity. In Section 3, the design method of the controller and law is presented to realize the finite-time robust feedback control of system (1). In Section 4, the circuit schematic diagram of the system (1) is given, and, by using an appropriate control circuit to realize the synchronization of master–slave systems, the reliability and existence of system (1) is verified by numerical simulation. The last section summarizes the dynamic analysis, control and circuit implementation, and gives prospects of future work.

## 2. Dynamical Properties

### 2.1. Equilibria and Stability

Let  $\dot{x}_1 = 0, \dot{x}_2 = 0, \dot{x}_3 = 0$ , its equilibria be  $S_1\left(\sqrt{\frac{b}{a}}, -\sqrt{ab}, 0\right), S_2\left(-\sqrt{\frac{b}{a}}, \sqrt{ab}, 0\right), S_3(0, x_2, x_3)$  and its Jacobian matrix be

$$J = \begin{pmatrix} x_2^2 + 2ax_1x_2 & 2x_1x_2 + ax_1^2 & 0 \\ -x_3 & 0 & -x_1 \\ b + 2x_1x_2 & x_1^2 & 0 \end{pmatrix} \tag{2}$$

Let  $|\lambda E - J| = 0$ , and obtain its characteristic equation as

$$f(\lambda) = \lambda^3 + A_2\lambda^2 + A_1\lambda + A_0 \tag{3}$$

From Equation (3),

$$\begin{aligned} A_2 &= -x_2^2 - 2ax_1x_2 \\ A_1 &= x_1^2 + ax_1^2x_3 + 2x_1x_2x_3 \\ A_0 &= -x_1^2x_2^2 - 2ax_1^3x_2 + 2bx_1^2x_2 + abx_1^3 + 4x_1^3x_2^2 + 2ax_1^4x_2 \end{aligned}$$

According to Routh–Hurwitz criterion, when  $A_2 > 0, A_0 > 0$  and  $A_2A_1 - A_0 > 0$ , the equilibrium is stable and is a stable point or stable point intersection; when  $A_2 > 0, A_0 > 0$  and  $A_2A_1 - A_0 < 0$ , the equilibrium point is a saddle.

### 2.2. Dynamical Behaviors Analysis

In system (1),  $x_1, x_2$  and  $x_3$  are state variables, and  $a$  and  $b$  are parameters. The dynamic characteristics of the system (1) depend on the variation in parameters  $a$  and  $b$ . When the parameters are set as  $a = 1.92$  and  $b = 1$ , and the initial state  $(x_1, x_2, x_3) = (0.87, 0.4, 0)$ , the system (1) shows chaos, and the phase orbit diagram is shown in Figure 1.

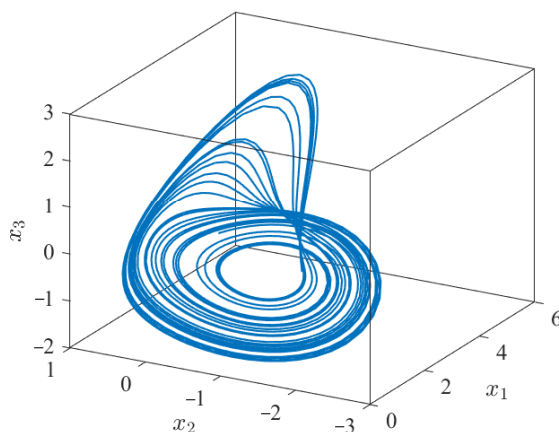


Figure 1. Chaos of system (1) with  $a = 1.92, b = 1$ .

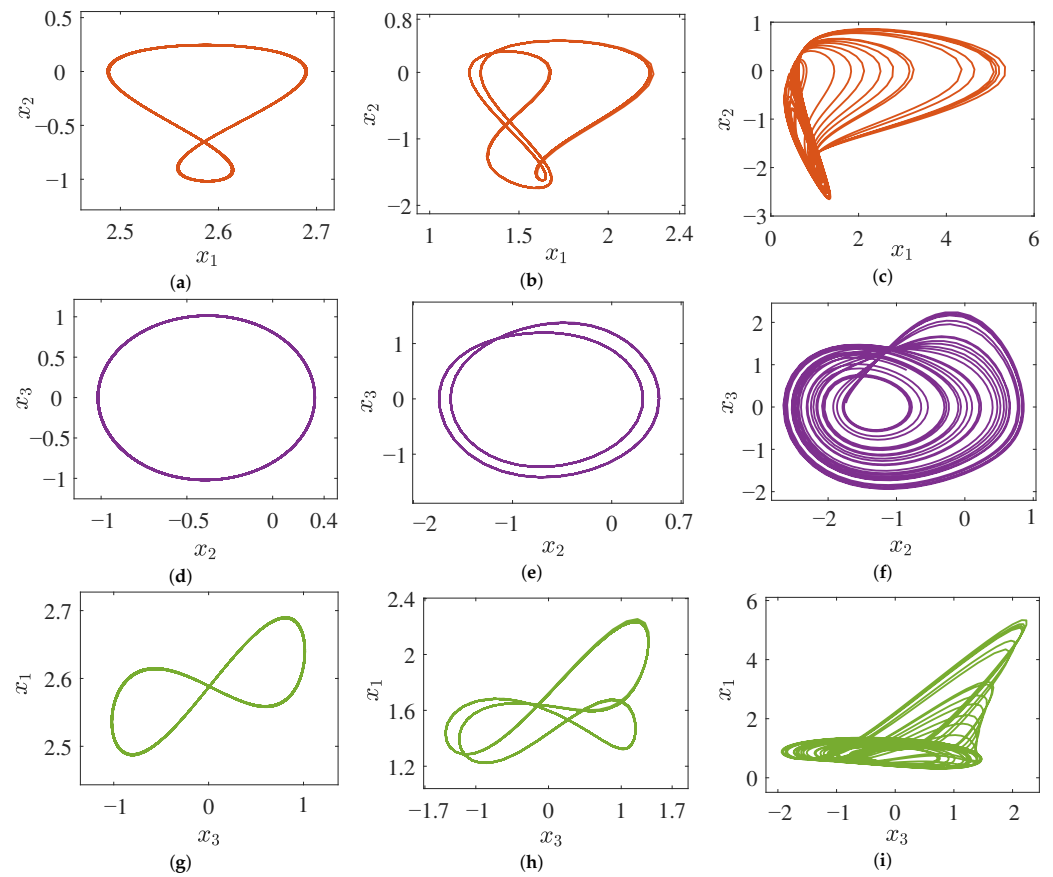
In order to study the dynamics of system (1), a numerical simulation is used and Table 1 shows the various phase diagrams of system (1) under different parameters.

Table 1. Dynamic behavior of the system (1) with different parameters (PVs, parameter values; PPs, phase portraits; Ps, Poincaré section).

PVs	Dynamics	LES	PPs	Ps
$a = 0.35$	Periodic-1	$[0, -0.1728, -0.1786]$	Figure 2a,d,g	Figure 3a
$a = 0.95$	Periodic-2	$[0, -0.0217, -0.1945]$	Figure 2b,e,h	Figure 3b
$a = 1.92$	Chaotic	$[0.0661, 0, -1.664]$	Figure 2c,f,i	Figure 3c

#### 2.2.1. Phase Orbits

The phase diagrams with periodic-1, periodic-2 and chaos can be obtained when the parameter  $b = 1$  is fixed and the parameter  $a$  is taken as 0.35, 0.95 and 1.92, respectively, as shown in Figure 2.



**Figure 2.** Periodic-1 and 2 and chaotic orbit of the system (1) with different  $a$ . (a)  $a = 0.35, b = 1$ . (b)  $a = 0.95, b = 1$ . (c)  $a = 1.92, b = 1$ . (d)  $a = 0.35, b = 1$ . (e)  $a = 0.95, b = 1$ . (f)  $a = 1.92, b = 1$ . (g)  $a = 0.35, b = 1$ . (h)  $a = 0.95, b = 1$ . (i)  $a = 1.92, b = 1$ .

2.2.2. Poincaré Section

The Poincaré section is used to take fixed values for the conjugate variables and intercept a plane in multiple dimensions. As shown in Figure 3, when the parameter  $a$  is chosen to be 0.35, 0.95 and 1.92, respectively, and the fixed parameter  $b = 1$ , the Poincaré section is in periodic-1, periodic-2 and chaos states in turn.

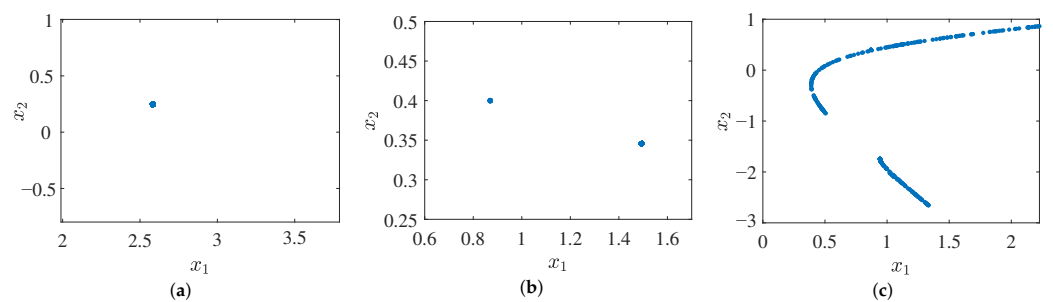


**Figure 3.** Periodic-1 and 2 and chaotic Poincaré surface of section of the system (1) with different  $a$ . (a)  $a = 0.35, b = 1$ . (b)  $a = 0.95, b = 1$ . (c)  $a = 1.92, b = 1$ .

From Figure 3, when parameter  $a$  is set to 0.35 or 0.95, the Poincaré region will only have one or two discrete points, indicating periodic behavior of the system (1), and, as the parameter  $a$  is set to 1.92, the Poincaré section is continuous with dense points, indicating that the system (1) exhibits chaos.

### 2.2.3. Lyapunov Exponent

For system (1), the Lyapunov dimension can be used to characterize the geometric properties of chaotic attractors. Its defining equation is:

$$D_\lambda = j + \frac{1}{|\lambda_{j+1}|} \sum_{i=1}^j \lambda_i \tag{4}$$

The above equation has a system dimension of  $D_\lambda = 2.040$  for  $a = 1.92$  and  $b = 1$ , and the system (1) has a fractal Lyapunov dimension, which shows the chaotic state. In order to confirm it, we need to fix the parameter  $b$ , change the parameter  $a$  and calculate the Lyapunov exponents spectrum of the system (1). The Lyapunov exponent spectrum of system (1) shown in Figure 4 fluctuates in the interval  $[0.5, 2.5]$ , whereas Figure 5 shows the largest Lyapunov exponent.

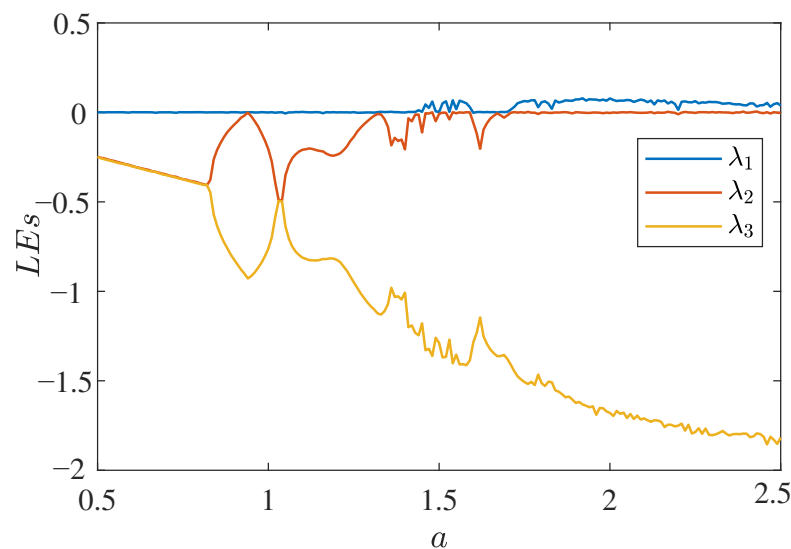


Figure 4. Lyapunov exponents spectrum (LEs) of the system (1) for  $b = 1$ .

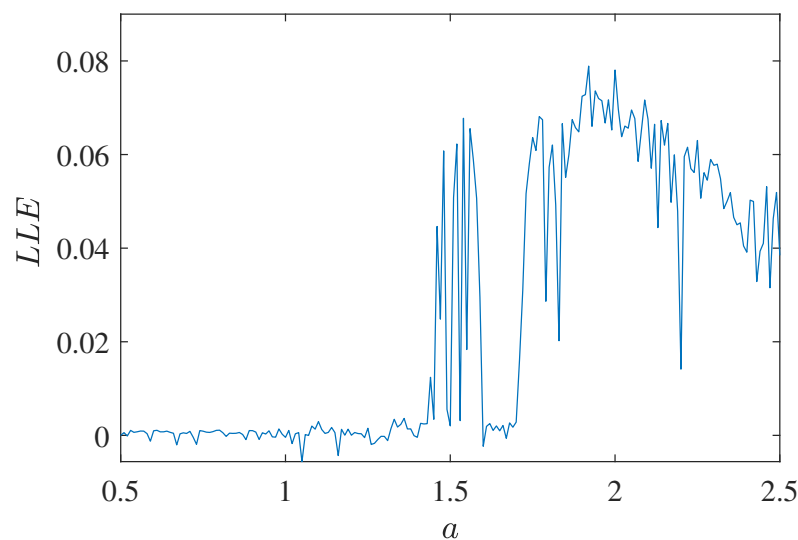
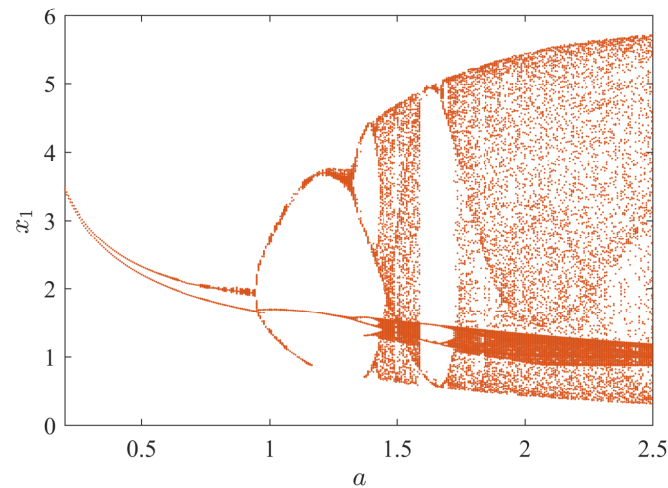


Figure 5. Largest Lyapunov exponent (LLE) of the system (1) for  $b = 1$ .

From Figure 5, the largest Lyapunov exponent  $\lambda_1 > 0$  is observed. This observation is also confirmed in Table 1.

#### 2.2.4. Bifurcation

A bifurcation diagram can also describe the chaotic states of system (1). Through the bifurcation state in Figure 6, the state of system (1) clearly changes from periodic to chaotic; then, combined with observing the Lyapunov exponents spectrum, it is found that system (1) changes its state when the parameter  $a$  changes, indicating that system (1) can only generate chaotic behavior within a certain parameter range.



**Figure 6.** Bifurcation of system (1) for  $b = 1$ .

According to the diagram above, parameter  $a$  can determine whether system (1) is in a chaotic state or periodic state. The complex dynamic behavior of system (1) can be controlled more easily by changing the value of  $a$ .

#### 2.2.5. Complexity Resolution

The complexity of system (1) is a measure of how similar a chaotic sequence is to a random sequence. The larger the complexity, the closer the sequence is to a random sequence. The spectral entropy complexity  $SE$  and complexity  $C_0$  with parameter  $a$  for  $b = 1$  are described in Figure 7 and Figure 8, respectively.

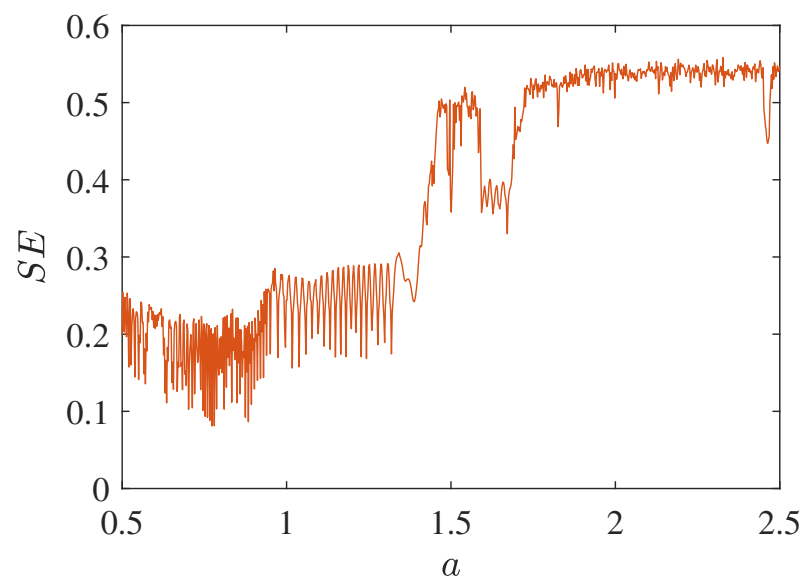


**Figure 7.** Complexity  $SE$  of system (1).

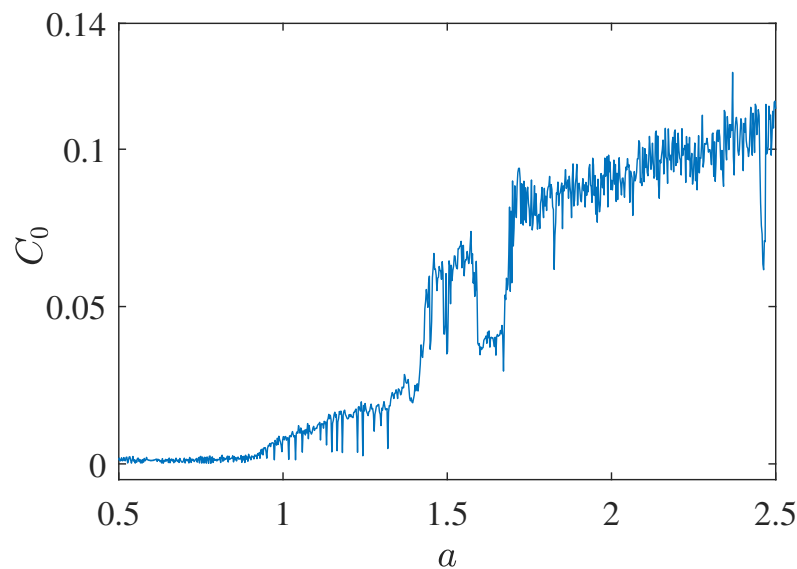


Figure 8. Complexity  $C_0$  of system (1).

The analysis of the complexity  $SE$  and the complexity  $C_0$  show that they are consistent with the Lyapunov exponents spectrum and the bifurcation diagram.

### 3. Design of Feedback Controller

#### 3.1. Implementation of Robust Controller

The master system of system (1) can be expressed as follows:

$$\begin{cases} \dot{x}_1 = x_1x_2^2 + (a + \Delta_1)x_1^2x_2 \\ \dot{x}_2 = -x_1x_3 \\ \dot{x}_3 = (b + \Delta_2)x_1 + x_1^2x_2 \end{cases} \quad (5)$$

where  $x = (x_1, x_2, x_3)^T$  is the state variable of the master system, and the slave system can be defined as

$$\begin{cases} \dot{y}_1 = y_1y_2^2 + (a + \Delta_3)y_1^2y_2 + u_1(t) \\ \dot{y}_2 = -y_1y_3 + u_2(t) \\ \dot{y}_3 = (b + \Delta_4)y_1 + y_1^2y_2 + u_3(t) \end{cases} \quad (6)$$

where  $y = (y_1, y_2, y_3)^T$  is the state variable of the slave system;  $\Delta_i$  ( $i = 1, 2, 3, 4$ ) is the parameter uncertainty of the master–slave chaotic system;  $u_i(t)$  ( $i = 1, 2, 3$ ) is the external input controller.

Define the master–slave error as  $e_i = y_i - x_i$  ( $i = 1, 2, 3$ ); through calculation, the error system is

$$\begin{cases} \dot{e}_1 = e_1y_2^2(1 + a(y_1 + x_1)) + x_1e_2((y_2 + x_2) + ax_1) \\ \quad + \Delta_3e_1y_1^2 + \Delta_1e_1x_1^2 + u_1(t) \\ \dot{e}_2 = -e_1y_3 - x_1e_3 + u_2(t) \\ \dot{e}_3 = (b - x_2(y_1 + x_1))e_1 + y_2^2e_2 + \Delta_4e_3 + \Delta_2e_3 + u_3(t) \end{cases} \quad (7)$$

Then, the robust feedback controller can be designed as

$$\begin{cases} u_1(t) = -e_1y_2^2(1 + a(y_1 + x_1)) - x_1e_2((y_2 + x_2) + ax_1) \\ \quad - \delta_3e_1y_1^2 - \delta_1e_1x_1^2 - k(|e_1|^{\xi_1})\text{sign}(e_1) \\ u_2(t) = e_1y_3 + x_1e_3 - k(|e_2|^{\xi_2})\text{sign}(e_2) \\ u_3(t) = -(b - x_2(y_1 - x_1))e_1 - y_2^2e_2 - \delta_4e_3 - \delta_2e_3 \\ \quad - k(|e_3|^{\xi_3})\text{sign}(e_3) \end{cases} \quad (8)$$

where  $0 < \xi_i < 1$  ( $i = 1, 2, 3$ ) and  $k > 0$ . To facilitate the computational discussion, the following lemmas and assumption are required.

**Lemma 1** ([42]). *When  $\alpha, \beta$  and  $\xi$  are all positive and  $0 < \xi < 1$ , then we have the inequality  $(\alpha + \beta)^\xi \leq \alpha^\xi + \beta^\xi$ .*

**Lemma 2** ([42]). *(Finite time stability) If continuous, positive definite  $V(t)$  satisfies*

$$\dot{V}(t) \leq -\varepsilon V^a(t), \forall t \geq t_0, V(t_0) \geq 0 \tag{9}$$

*Among them,  $\varepsilon > 0$  and  $0 < a < 1$ ; then, for any given  $t_0$ ,  $V(t)$  satisfies the following differential inequality:*

$$V^{1-a}(t) \leq V^{1-a}(t_0) - \varepsilon(1-a)(t-t_0), t_0 \leq t \leq t_{fin} \tag{10}$$

*and, when  $\forall t \geq t_{fin}$ , there are  $V(t) = 0$ ; among them,  $t_{fin} = t_0 + \frac{V^{1-a}(t_0)}{\varepsilon(1-a)}$ .*

Suppose that there exists a positive number  $\delta_i$  ( $i = 1, 2, 3 \dots$ ); make the parameter perturbation  $|\Delta_i| \leq \delta_i$  ( $i = 1, 2, 3 \dots$ ).

### 3.2. Performance of Robust Feedback Controller

After constructing systems (5) and (6) using the robust feedback controller (8), we have the following theorem:

**Theorem 1.** *For system (5) and system (6), the controller (8) is used, and  $0 < \xi_i < 1$  ( $i = 1, 2, 3$ ). Through Lemma 2, the finite-time  $T = t_0 + \frac{2^{\sigma-1}V^\sigma(t_0)}{\sigma}$ , and then master-slave systems tend to be synchronized, where  $\sigma = \frac{1-\xi}{2}$ .*

**Proof.** Construct the Lyapunov function  $V(t) = \frac{1}{2} \sum_{i=1}^3 e_i^2$ , on the derivation of time  $t$ ;  $\dot{V}(t) = \sum_{i=1}^3 e_i \cdot \dot{e}_i$  is available.

Substituting the three error systems (7) into the above equation, we can obtain

$$\begin{aligned} \dot{V}(t) &= e_1 \dot{e}_1 + e_2 \dot{e}_2 + e_3 \dot{e}_3 \\ &= e_1 \left( e_1 y_2^2 (1 + a(y_1 + x_1)) + x_1 e_2 ((y_2 + x_2) + a x_1) \right) \\ &\quad + e_1 \left( \Delta_3 e_1 y_1^2 + \Delta_1 e_1 x_1^2 + u_1(t) \right) \\ &\quad + e_2 \left( -e_1 y_3 - x_1 e_3 + u_2(t) \right) + e_3 \left( (b - x_2(y_1 + x_1)) e_1 \right) \\ &\quad + e_3 \left( y_2^2 e_2 + \Delta_4 e_3 + \Delta_2 e_3 + u_3(t) \right) \end{aligned} \tag{11}$$

The robust feedback controller (8) is substituted into the above Equation (11), and terms are cancelled, to obtain

$$\begin{aligned} \dot{V}(t) &= e_1 \left( \Delta_3 e_1 y_1^2 + \Delta_1 e_1 x_1^2 \right) \\ &\quad + e_1 \left( -\delta_3 e_1 y_1^2 - \delta_1 e_1 x_1^2 - k \left( |e_1|^{\xi_1} \right) \text{sign}(e_1) \right) \\ &\quad + e_2 \left( -k \left( |e_2|^{\xi_2} \right) \text{sign}(e_2) \right) \\ &\quad + e_3 \left( -\delta_4 e_3 - \delta_2 e_3 - k \left( |e_3|^{\xi_3} \right) \text{sign}(e_3) \right) \\ &\quad + e_3 \left( \Delta_4 e_3 + \Delta_2 e_3 \right) \end{aligned} \tag{12}$$

and, then, one can further obtain:

$$\begin{aligned} \dot{V}(t) &= \Delta_3 e_1^2 y_1^2 - \delta_3 e_1^2 y_1^2 + \Delta_1 e_1^2 x_1^2 - \delta_1 e_1^2 x_1^2 + \Delta_4 e_3^2 - \delta_4 e_3^2 + \Delta_2 e_3^2 - \delta_2 e_3^2 \\ &\quad - k(|e_1|^{\xi_1})|e_1| - k(|e_2|^{\xi_2})|e_2| - k(|e_3|^{\xi_3})|e_3| \\ &= e_1^2 y_1^2 (\Delta_3 - \delta_3) + e_1^2 x_1^2 (\Delta_1 - \delta_1) + e_3^2 (\Delta_4 - \delta_4) + e_3^2 (\Delta_2 - \delta_2) \\ &\quad - k(|e_1|^{\xi_1})|e_1| - k(|e_2|^{\xi_2})|e_2| - k(|e_3|^{\xi_3})|e_3| \end{aligned} \tag{13}$$

From Assumption 1, from the existence of positive numbers  $\delta_i (i = 1, 2, 3 \dots)$ ,  $|\Delta_i| \leq \delta_i (i = 1, 2, 3 \dots)$ ,

$$e_1^2 y_1^2 (\Delta_3 - \delta_3) + e_1^2 x_1^2 (\Delta_1 - \delta_1) + e_3^2 (\Delta_4 - \delta_4) + e_3^2 (\Delta_2 - \delta_2) \leq 0 \tag{14}$$

According to  $\zeta$ , we have  $\dot{V}(t) \leq -k(|e_1|^{\xi+1}) - k(|e_2|^{\xi+1}) - k(|e_3|^{\xi+1})$ . Combined with Lemma 1, we have

$$\begin{aligned} &-k(|e_1|^{\xi+1}) - k(|e_2|^{\xi+1}) - k(|e_3|^{\xi+1}) \\ &= -2^{\frac{\xi+1}{2}} k \left( \left( \frac{(|e_1|)^2}{2} \right)^{\frac{\xi+1}{2}} \right) + \left( \left( \frac{(|e_2|)^2}{2} \right)^{\frac{\xi+1}{2}} \right) + \left( \left( \frac{(|e_3|)^2}{2} \right)^{\frac{\xi+1}{2}} \right) \\ &\leq -2^{\frac{\xi+1}{2}} k \left( \frac{(|e_1|)^2}{2} + \frac{(|e_2|)^2}{2} + \frac{(|e_3|)^2}{2} \right)^{\frac{\xi+1}{2}} \end{aligned} \tag{15}$$

It is clear that  $\dot{V}(t) \leq -2^{\frac{\xi+1}{2}} k V^{\frac{\xi+1}{2}}(t)$ .

From Lemma 2, it is known that there exists

$$T = t_0 + \frac{V^{1-\frac{\xi+1}{2}}(t_0)}{2^{\frac{\xi+1}{2}} K \left(1 - \frac{\xi+1}{2}\right)} = t_0 + \frac{2^{\frac{1-\xi}{2}} k V^{\frac{1-\xi}{2}}(t_0)}{1 - \zeta} \tag{16}$$

and let  $\sigma = (1 - \zeta)/2$ ; at finite time  $T = t_0 + \frac{2^{\sigma-1} V(t_0)}{\sigma}$ , the system containing parameter uncertainty achieves finite-time synchronization, where  $e_i \rightarrow 0 (i = 1, 2, 3)$  at  $t \geq T$ . This completes the proof.  $\square$

### 3.3. Numerical Simulation

For a master-slave system with parameters  $a = 1.92, b = 1$  and  $\Delta_i = 0 (i = 1, 2, 3, 4)$ , the system is in a chaotic state. The master-slave system applies a system controller with parameters taken as  $\Delta_1 = 0.08 \sin(t), \Delta_2 = 0.08 \sin(t), \Delta_3 = 0.08 \sin(t)$  and  $\Delta_4 = 0.08 \sin(t)$ ; then, it is known that  $\delta_1 = 1, \delta_2 = 1$  and  $\delta_3 = 1, \delta_4 = 1$ . The control parameters are taken as  $\zeta_1 = 0.5, \zeta_2 = 0.5$  and  $\zeta_3 = 0.5$ , and the orbits of the states of the master and slave systems are shown in Figure 9.

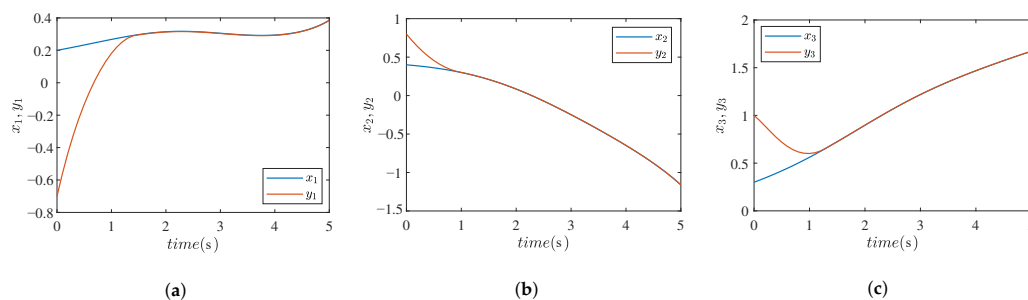


Figure 9. Synchronization of master-slave system. (a)  $x_1, y_1$ . (b)  $x_2, y_2$ . (c)  $x_3, y_3$ .

From Figure 9, the states of the master–slave system tend to converge, and synchronization errors are demonstrated in Figure 10.

From the simulation result in Figure 10, it can be seen that the trajectory of the synchronization error system converges asymptotically to the origin. In addition, Figures 9 and 10 illustrate the control effect of the designed controller.

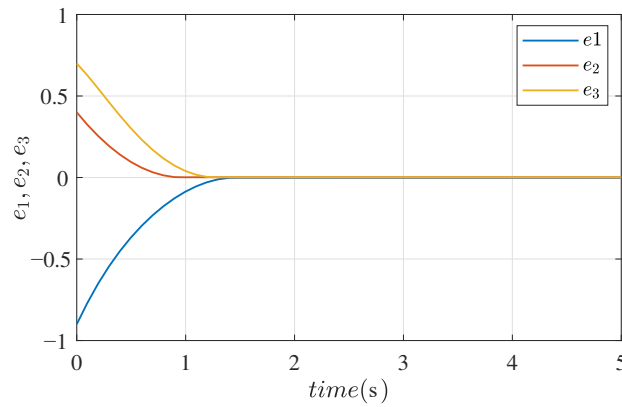


Figure 10. Time responses of the synchronization errors.

#### 4. Circuit Implementation and Numerical Simulation

##### 4.1. Circuit Implementation

We used the operational amplifier LM741, analog multiplier AD633, resistors and capacitors to design the analog circuit. The power voltage of the operational amplifier LM741 is  $\pm 15$  V, and its output saturation voltage is  $V_{sat} \approx \pm 13.5$  V. According to system (5), a chaotic circuit was designed, as shown in Figure 11.

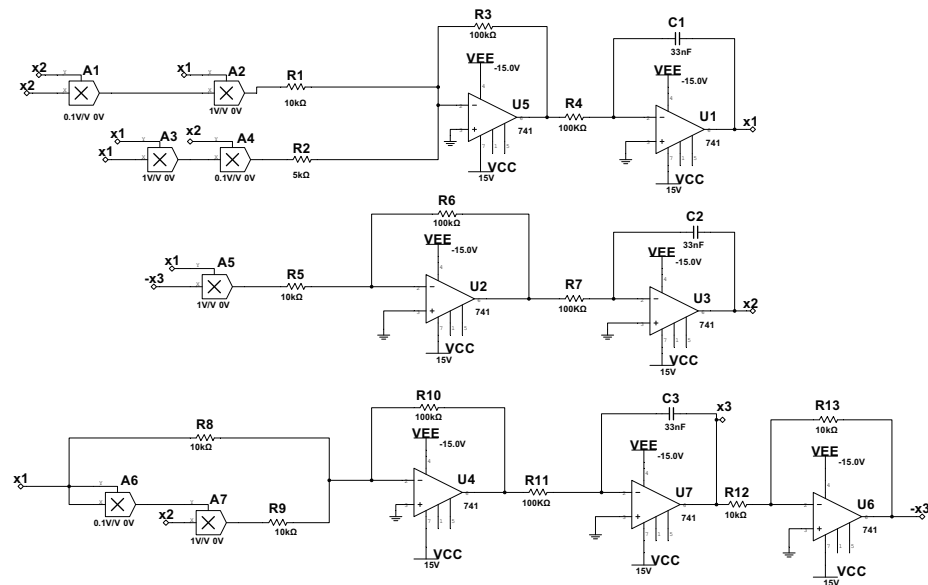


Figure 11. Analog circuit of the system (1).

From Figure 11, applying Kirchhoff’s law, the corresponding circuit equations can be listed as

$$\begin{cases} \frac{dx_1}{dt} = \frac{R_3}{R_1} \frac{1}{c_1 R_4} (-x_1)x_2^2 + \frac{R_3}{R_2} \frac{1}{c_1 R_4} (-x_2)x_1^2 \\ \frac{dx_2}{dt} = \frac{R_6}{R_5} \frac{1}{c_2 R_7} (-x_1)x_3 \\ \frac{dx_3}{dt} = \frac{R_{14}}{R_{15}} \frac{R_{10}}{R_8} \frac{1}{c_3 R_{12}} (-x_1) + \frac{R_{14}}{R_{15}} \frac{R_{10}}{R_9} \frac{1}{c_3 R_{12}} (-x_2)x_1^2 \end{cases} \quad (17)$$

where  $x_1$ ,  $x_2$  and  $x_3$  are related to the voltage on the capacitors, respectively.

4.2. Circuit Simulation

For circuit system (17), capacitor  $C1 = C2 = C3 = 33 \text{ nf}$ , resistance  $R2 = 5 \text{ k}\Omega$ ,  $R1 = R5 = R8 = R9 = R12 = R13 = 10 \text{ k}\Omega$ ,  $R3 = R4 = R6 = R7 = R10 = R11 = 100 \text{ k}\Omega$  can be obtained. The gain in the AD633 multiplier  $A1 = A4 = A6 = 0.1$  and  $A2 = A3 = A5 = A7 = 1$ . According to the above circuit parameters, the phase diagram shown in Figure 12 can be obtained on a digital oscilloscope.

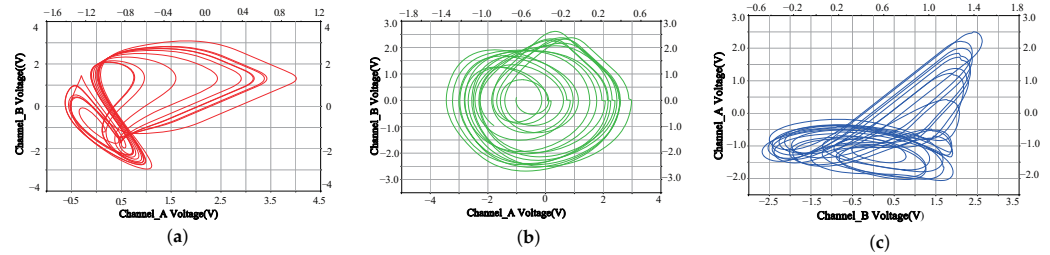


Figure 12. Analog circuit simulation phase results of system (1). (a)  $x_1 - x_2$ . (b)  $x_2 - x_3$ . (c)  $x_3 - x_1$ .

These results are consistent with the results of the numerical simulation and analog circuit simulation, which proves that the digital circuit can verify the chaotic behavior of this system. These numerical simulations are performed to verify the correctness of the system (1).

After realizing the above circuit simulation, in order to further achieve a synchronous circuit, the master system selects the chaotic system proposed in this paper, and system (1) can be rewritten as follows:

$$\begin{cases} \dot{x}_{m1} = x_1x_2^2 + ax_1^2x_2 - k_1(x_{m1} - x_1) \\ \dot{x}_{m2} = -x_1x_3 - k_2(x_{m2} - x_2) \\ \dot{x}_{m3} = bx_1 + x_1^2x_2 - k_3(x_{m3} - x_3) \end{cases} \quad (18)$$

where the parameters of the drive system are  $a = 1.92$ ,  $b = 1$ ,  $k_1 = 1$ ,  $k_2 = 22$  and  $k_3 = 22$ . The state vector is  $x = [x_{m1}, x_{m2}, x_{m3}]^T$ . The schematic diagram of the synchronization circuit and synchronization phase diagram are shown in Figures 13 and 14. In addition, from Figure 14, it can be seen from the three phase planes that the master–slave system can achieve synchronization.

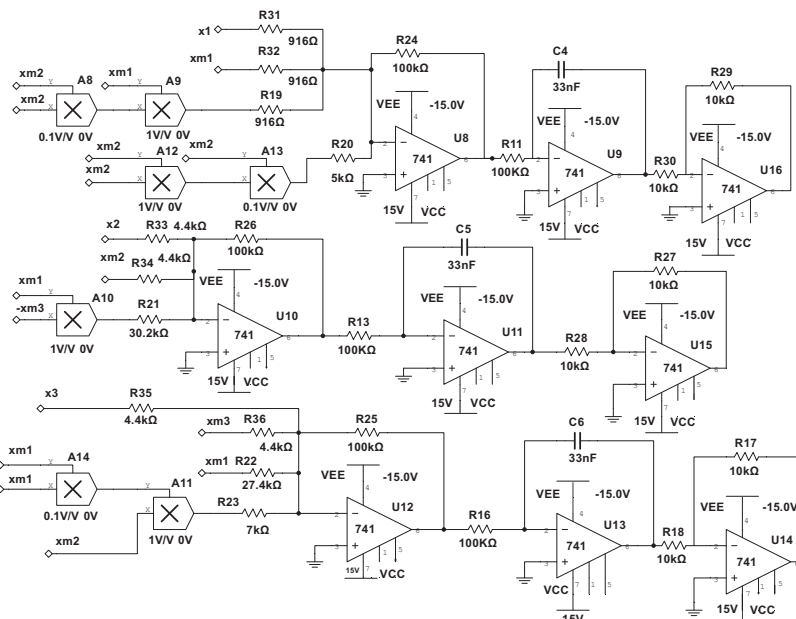
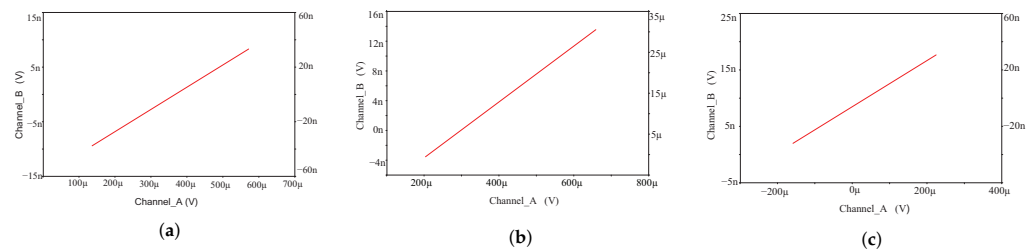


Figure 13. Schematic diagram of synchronization analog circuit of system (1).



**Figure 14.** Analog circuit simulation results of system (1). (a)  $x_1, x_{m1}$ . (b)  $x_2, x_{m2}$ . (c)  $x_3, x_{m3}$ .

## 5. Conclusions

In this paper, we analyzed the dynamical behavior of a surface equilibrium system with a hidden attractor (including phase analysis, Lyapunov exponent, bifurcation, Poincaré section, complexity, etc.). Moreover, a finite-time robust feedback controller was proposed for the synchronization and control problem of the surface equilibrium system with a hidden attractor, and the synchronization of master–slave systems in finite time was realized. Furthermore, a simulation circuit was designed to implement the system model, and the circuit synchronization simulation of the master–slave system was realized. The experimental results of the circuit are consistent with the simulation results of the theoretical model. Finally, in future work, we will find a better controller and implement its circuit, and a more comprehensive dynamic analysis of the system can also be carried out. By studying the latest results, the control method can also be further improved.

**Author Contributions:** Supervision, Z.W.; writing—visualization, H.T.; writing—original draft, R.Z.; writing—review and editing, X.X., H.T. and Z.W. All authors have read and agreed to the published version of the manuscript.

**Funding:** This work is supported by the National Natural Science Foundation of China (61973249), the Key Research and Development programs of Shaanxi Province (2021ZDLGY02-06), the Natural Science Basic Research Program of Shaanxi (2021JM-533, 2021JQ-880, 2020JM-646, 2021JQ-868), the Innovation Capability Support Program of Shaanxi (2018GHJD-21), the Qin Chuangyuan Project (2021QCYRC4-49), the Support Plan for Sanqin Scholars Innovation Team in Shaanxi Province of China, the National Defense Science and Technology Key Laboratory Fund Project (6142101210202), the Qinchuangyuan Scientist+Engineer (2022KXJ-169), the Scientific Research Program Funded by Shaanxi Provincial Education Department (21JK0960) and the Scientific Research Foundation of Xijing University (XJ210203).

**Data Availability Statement:** Not applicable.

**Acknowledgments:** The author acknowledges the referees and the editor for carefully reading this paper and giving many helpful comments. The authors also express their gratitude to the reviewers for their insightful comments.

**Conflicts of Interest:** The authors declare no conflict of interest.

## References

1. Kapitaniak, T.; Jafari, S. Nonlinear effects in life sciences. *Eur. Phys. J. Spec. Top.* **2018**, *227*, 693–696. [[CrossRef](#)]
2. Lorenz, E.N. Deterministic nonperiodic flow. *J. Atmos. Sci.* **1963**, *20*, 130–141. [[CrossRef](#)]
3. Sprott, J.C. Some simple chaotic flows. *Phys. Rev. E* **1994**, *50*, R647. [[CrossRef](#)] [[PubMed](#)]
4. Chen, G.; Ueta, T. Yet another chaotic attractor. *Int. J. Bifurc. Chaos* **1999**, *9*, 1465–1466. [[CrossRef](#)]
5. Lü, J.; Chen, G. A new chaotic attractor coined. *Int. J. Bifurc. Chaos* **2002**, *12*, 659–661. [[CrossRef](#)]
6. Leonov, G.A.; Kuznetsov, N.V. *Algorithms for Searching for Hidden Oscillations in the Aizerman and Kalman Problems*; Springer: Berlin/Heidelberg, Germany, 2011.
7. Tian, H.; Wang, Z.; Zhang, H.; Cao, Z.; Zhang, P. Dynamical analysis and fixed-time synchronization of a chaotic system with hidden attractor and a line equilibrium. *Eur. Phys. J. Spec. Top.* **2022**, *231*, 2455–2466. [[CrossRef](#)]
8. Leonov, G.A.; Kuznetsov, N.V. Hidden attractors in dynamical systems. From hidden oscillations in Hilbert–Kolmogorov, Aizerman, and Kalman problems to hidden chaotic attractor in Chua circuits. *Int. J. Bifurc. Chaos* **2013**, *23*, 1330002. [[CrossRef](#)]
9. Dudkowski, D.; Jafari, S.; Kapitaniak, T.; Kuznetsov, N.V.; Leonov, G.A.; Prasad, A. Hidden attractors in dynamical systems. *Phys. Rep.* **2016**, *637*, 1–50. [[CrossRef](#)]

10. Wang, Z.; Wei, Z.; Sun, K.; He, S.; Wang, H.; Xu, Q.; Chen, M. Chaotic flows with special equilibria. *Eur. Phys. J. Spec. Top.* **2020**, *229*, 905–919. [[CrossRef](#)]
11. Wang, X.; Chen, G. A chaotic system with only one stable equilibrium. *Commun. Nonlinear Sci. Numer. Simul.* **2012**, *17*, 1264–1272. [[CrossRef](#)]
12. Deng, Q.; Wang, C.; Yang, L. Four-wing hidden attractors with one stable equilibrium point. *Int. J. Bifurc. Chaos* **2020**, *30*, 2050086. [[CrossRef](#)]
13. Wei, Z. Dynamical behaviors of a chaotic system with no equilibria. *Phys. Lett. A* **2011**, *376*, 102–108. [[CrossRef](#)]
14. Jafari, S.; Sprott, J.C.; Golpayegani, S.M.R.H. Elementary quadratic chaotic flows with no equilibria. *Phys. Lett. A* **2013**, *377*, 699–702. [[CrossRef](#)]
15. Li, C.; Sprott, J.C.; Thio, W. Bistability in a hyperchaotic system with a line equilibrium. *J. Exp. Theor. Phys.* **2014**, *118*, 494–500. [[CrossRef](#)]
16. Li, Q.; Hu, S.; Tang, S.; Zeng, G. Hyperchaos and horseshoe in a 4D memristive system with a line of equilibria and its implementation. *Int. J. Circuit Theory Appl.* **2014**, *42*, 1172–1188. [[CrossRef](#)]
17. Kingni, S.T.; Pham, V.T.; Jafari, S.; Kol, G.R.; Woaf, P. Three-dimensional chaotic autonomous system with a circular equilibrium: Analysis, circuit implementation and its fractional-order form. *Circuits, Syst. Signal Process.* **2016**, *35*, 1933–1948. [[CrossRef](#)]
18. Kapitaniak, T.; Leonov, G.A. Multistability: Uncovering hidden attractors. *Eur. Phys. J. Spec. Top.* **2015**, *224*, 1405–1408. [[CrossRef](#)]
19. Wang, N.; Zhang, G.; Kuznetsov, N.V.; Bao, H. Hidden attractors and multistability in a modified Chua's circuit. *Commun. Nonlinear Sci. Numer. Simul.* **2021**, *92*, 105494. [[CrossRef](#)]
20. Yang, Y.; Qi, G.; Hu, J.; Faradja, P. Finding method and analysis of hidden chaotic attractors for plasma chaotic system from physical and mechanistic perspectives. *Int. J. Bifurc. Chaos* **2020**, *30*, 2050072. [[CrossRef](#)]
21. Wang, Z.; Baruni, S.; Parastesh, F.; Jafari, S.; Ghosh, D.; Perc, M.; Hussain, I. Chimeras in an adaptive neuronal network with burst-timing-dependent plasticity. *Neurocomputing* **2020**, *406*, 117–126. [[CrossRef](#)]
22. Wang, Z.; Parastesh, F.; Rajagopal, K.; Hamarash, I.I.; Hussain, I. Delay-induced synchronization in two coupled chaotic memristive Hopfield neural networks. *Chaos Solitons Fractals* **2020**, *134*, 109702. [[CrossRef](#)]
23. Liang, H.; Wang, Z.; Yue, Z.; Lu, R. Generalized synchronization and control for incommensurate fractional unified chaotic system and applications in secure communication. *Kybernetika* **2012**, *48*, 190–205.
24. Xi, X.; Mobayen, S.; Ren, H.; Jafari, S. Robust finite-time synchronization of a class of chaotic systems via adaptive global sliding mode control. *J. Vib. Control* **2018**, *24*, 3842–3854. [[CrossRef](#)]
25. Ghosh, D. Nonlinear-observer-based synchronization scheme for multiparameter estimation. *EPL (Europhys. Lett.)* **2008**, *84*, 40012. [[CrossRef](#)]
26. Chaudhary, H.; Khan, A.; Nigar, U.; Kaushik, S.; Sajid, M. An Effective Synchronization Approach to Stability Analysis for Chaotic Generalized Lotka–Volterra Biological Models Using Active and Parameter Identification Methods. *Entropy* **2022**, *24*, 529. [[CrossRef](#)]
27. Sun, J.; Wang, Y.; Wang, Y.; Shen, Y. Finite-time synchronization between two complex-variable chaotic systems with unknown parameters via nonsingular terminal sliding mode control. *Nonlinear Dyn.* **2016**, *85*, 1105–1117. [[CrossRef](#)]
28. Deng, Y.; Hu, H.; Xiong, W.; Xiong, N.N.; Liu, L. Analysis and design of digital chaotic systems with desirable performance via feedback control. *IEEE Trans. Syst. Man Cybern. Syst.* **2015**, *45*, 1187–1200. [[CrossRef](#)]
29. Ghosh, D.; Banerjee, S. Adaptive scheme for synchronization-based multiparameter estimation from a single chaotic time series and its applications. *Phys. Rev. E* **2008**, *78*, 056211.
30. Ghosh, D.; Frasca, M.; Rizzo, A.; Majhi, S.; Rakshit, S.; Alfaro-Bittner, K.; Boccaletti, S. The synchronized dynamics of time-varying networks. *Phys. Rep.* **2022**, *949*, 1–63. [[CrossRef](#)]
31. Chen, W.; Zhang, R.; Zhao, L.; Wang, H.; Wei, Z. Control of chaos in vehicle lateral motion using the sliding mode variable structure control. *Proc. Inst. Mech. Eng. Part J. Automob. Eng.* **2019**, *233*, 776–789. [[CrossRef](#)]
32. Wang, C.; Tang, J.; Jiang, B.; Wu, Z. Sliding-mode variable structure control for complex automatic systems: A survey. *Math. Biosci. Eng.* **2022**, *19*, 2616–2640. [[CrossRef](#)]
33. Liu, J.; Wang, Z.; Chen, M.; Zhang, P.; Yang, R.; Yang, B. Chaotic system dynamics analysis and synchronization circuit realization of fractional-order memristor. *Eur. Phys. J. Spec. Top.* **2022**, 1–13. [[CrossRef](#)]
34. Tian, H.; Wang, Z.; Zhang, P.; Chen, M.; Wang, Y. Dynamic analysis and robust control of a chaotic system with hidden attractor. *Complexity* **2021**, *2021*, 8865522. [[CrossRef](#)]
35. Haimo, V.T. Finite time controllers. *SIAM J. Control Optim.* **1986**, *24*, 760–770. [[CrossRef](#)]
36. Yu, S.; Yu, X.; Zhihong, M. Robust global terminal sliding mode control of SISO nonlinear uncertain systems. In *Proceedings of the Proceedings of the 39th IEEE Conference on Decision and Control (Cat. No. 00CH37187), Sydney, Australia, 12–15 December 2000*; IEEE: Piscataway, NJ, USA, 2000; Volume 3, pp. 2198–2203.
37. Amato, F.; Ariola, M.; Dorato, P. Finite-time control of linear systems subject to parametric uncertainties and disturbances. *Automatica* **2001**, *37*, 1459–1463. [[CrossRef](#)]
38. Li, S.; Tian, Y. Finite time synchronization of chaotic systems. *Chaos Solitons Fractals* **2003**, *15*, 303–310. [[CrossRef](#)]
39. Perruquetti, W.; Floquet, T.; Moulay, E. Finite-time observers: Application to secure communication. *IEEE Trans. Autom. Control* **2008**, *53*, 356–360. [[CrossRef](#)]
40. Wang, H.; Ye, J.; Miao, Z.; Jonckheere, E.A. Robust finite-time chaos synchronization of time-delay chaotic systems and its application in secure communication. *Trans. Inst. Meas. Control* **2018**, *40*, 1177–1187. [[CrossRef](#)]

41. Jafari, S.; Sprott, J.C.; Pham, V.T.; Volos, C.; Li, C. Simple chaotic 3D flows with surfaces of equilibria. *Nonlinear Dyn.* **2016**, *86*, 1349–1358. [[CrossRef](#)]
42. Aghababa, M.P.; Khanmohammadi, S.; Alizadeh, G. Finite-time synchronization of two different chaotic systems with unknown parameters via sliding mode technique. *Appl. Math. Model.* **2011**, *35*, 3080–3091. [[CrossRef](#)]